ELSEVIER

NeuroImage

www.elsevier.com/locate/ynimg
NeuroImage 26 (2005) 243–250

Comparison of physiological noise at 1.5 T, 3 T and 7 T and optimization of fMRI acquisition parameters

C. Triantafyllou,[a,*] R.D. Hoge,[a] G. Krueger,[b] C.J. Wiggins,[a] A. Potthast,[b] G.C. Wiggins,[a] and L.L. Wald[a]

[a]*MGH/MIT/HMS A.A. Martinos Center for Biomedical Imaging, Massachusetts General Hospital, Department of Radiology, Building 149, 13th Street, Charlestown, MA 02129, USA*
[b]*Siemens Medical Solutions, Henkestr 127, 91052 Erlangen, Germany*

Received 24 September 2004; revised 9 December 2004; accepted 8 January 2005
Available online 3 March 2005

Previous studies have shown that under some conditions, noise fluctuations in an fMRI time-course are dominated by physiological modulations of the image intensity with secondary contributions from thermal image noise and that these two sources scale differently with signal intensity, susceptibility weighting (TE) and field strength. The SNR of the fMRI time-course was found to be near its asymptotic limit for moderate spatial resolution measurements at 3 T with only marginal gains expected from acquisition at higher field strengths. In this study, we investigate the amplitude of image intensity fluctuations in the fMRI time-course at magnetic field strengths of 1.5 T, 3 T, and 7 T as a function of image resolution, flip angle and TE. The time-course SNR was a similar function of the image SNR regardless of whether the image SNR was modulated by flip angle, image resolution, or field strength. For spatial resolutions typical of those currently used in fMRI (e.g., 3 × 3 × 3 mm^3), increases in image SNR obtained from 7 T acquisition produced only modest increases in time-course SNR. At this spatial resolution, the ratio of physiological noise to thermal image noise was 0.61, 0.89, and 2.23 for 1.5 T, 3 T, and 7 T. At a resolution of 1 × 1 × 3 mm^3, however, the physiological to thermal noise ratio was 0.34, 0.57, and 0.91 for 1.5 T, 3 T and 7 T for TE near T2*. Thus, by reducing the signal strength using higher image resolution, the ratio of physiologic to image noise could be reduced to a regime where increased sensitivity afforded by higher field strength still translated to improved SNR in the fMRI time-series.

Keywords: fMRI; Physiological noise; SNR; Magnetic field strength; 7 Tesla

Introduction

Magnetic resonance scanners operating at magnetic fields of 3 T and above have recently become widespread, partially due to increases in image signal-to-noise ratio (SNR) (Edelstein et al., 1986) and BOLD contrast at higher field (Bandettini et al., 1994; Gati et al., 1997; Turner et al., 1993). One of the primary motivations for the development of scanners with field strengths as high as 7 and 8 T has been to extend the boundaries of signal-to-noise ratio (SNR), spatial resolution, and sensitivity. However, in functional MRI, sensitivity is restricted by multiple sources of variance, such as instrumental sources of error including thermal noise and shot-to-shot electronic instability, and subject dependent modulations of the MR signal-associated with physiological processes. In addition to respiratory and cardiac cycle contributions, the physiological noise also consists of a noise element with BOLD-like TE dependence (Krueger and Glover, 2001), and spatial correlation within gray matter (Krueger and Glover, 2001; Weisskoff et al., 1993). The origin of this "BOLD noise" is still not fully understood, but is generally associated with hemodynamic and metabolic fluctuations in the gray matter.

Since the physiological fluctuations represent a multiplicative modulation of the image signal (Krueger and Glover, 2001), their amplitude scales with the MR image intensity. This is in contrast to the thermal noise sources which can be represented by the addition of a fixed amount of Gaussian noise power whose amplitude is determined primarily by the coil loading. The scaling of the physiological noise sources with field strength has been implicated as a possible cause of the less than linear increase in fMRI contrast to noise between 1.5 T and 3 T (Fera et al., 2004).

If the noise sources are assumed to be uncorrelated, the total noise in the image time-course (σ) is related to its thermal (σ_0) and physiological (σ_p) components via:

$$\sigma = \sqrt{\sigma_0^2 + \sigma_p^2}, \quad (1)$$

In our measurement, shot-to-shot scanner instabilities will contribute to both terms, σ_0 and σ_p, depending on their signal dependence. Phantom measurements, however, show that they comprise only a small fraction of the in vivo time series noise.

* Corresponding author. Fax: +1 617 726 7422.
E-mail address: christin@nmr.mgh.harvard.edu (C. Triantafyllou).
Available online on ScienceDirect (www.sciencedirect.com).

1053-8119/$ - see front matter © 2005 Elsevier Inc. All rights reserved.
doi:10.1016/j.neuroimage.2005.01.007

The time-course SNR (tSNR) is then defined as:

$$\mathrm{tSNR} = \frac{\bar{S}}{\sqrt{\sigma_0^2 + \sigma_\mathrm{p}^2}}, \tag{2}$$

where $\bar{S}$ is the mean image signal intensity. Defining the SNR in an individual image as $\mathrm{SNR}_0 = \frac{\bar{S}}{\sigma_0}$ and combining with Eq. (2), allows the ratio of physiological noise to thermal noise to be determined from a measurement of tSNR and SNR_0:

$$\frac{\sigma_\mathrm{p}}{\sigma_0} = \sqrt{\left(\frac{\mathrm{SNR}_0}{\mathrm{tSNR}}\right)^2 - 1}, \tag{3}$$

If the physiological variance, σ_p, is broken into BOLD-like (σ_B proportional to $\Delta R_2^* \times \mathrm{TE} \times S$) and non-BOLD ($\sigma_\mathrm{NB}$ proportional to S) components, each of which is proportional to the signal strength, S, then Eq. (1) can be rewritten as:

$$\sigma = \sqrt{\sigma_0^2 + \sigma_\mathrm{B}^2 + \sigma_\mathrm{NB}^2}, \qquad \text{(Krueger and Glover, 2001) or}$$

$$\sigma = \sqrt{\sigma_0^2 + \left(c_1 \times \Delta R_2^* \times \mathrm{TE} \times S\right)^2 + (c_2 \times S)^2}, \tag{4}$$

The relationship between tSNR and image SNR_0 is then given by the equation:

$$\mathrm{tSNR} = \frac{\mathrm{SNR}_0}{\sqrt{1 + \lambda^2 \times \mathrm{SNR}_0^2}}, \tag{5}$$

where $\lambda = \sqrt{c_1^2 \times \Delta R_2^{*2} \times \mathrm{TE}^2 + c_2^2}$. By plotting tSNR as a function of SNR_0 for different sets of scan parameters which produced differing SNR_0, the constant λ can be determined by fitting the data to Eq. (5). The constant λ is expected to be roughly independent of field strength (Krueger et al., 2001). As SNR_0 is increased, eventually, the tSNR reaches the asymptotic limit of $1/\lambda$. As this limit is approached, further increases in SNR_0 obtained by lowering the image resolution, improving the RF detectors, or increasing the static field strength yields only small increases in tSNR.

If SNR_0 is assumed to be proportional to voxel volume, V, with proportionality constant κ, then the relationship between tSNR and V can be written as:

$$\mathrm{tSNR} = \frac{\kappa \times V}{\sqrt{1 + \lambda^2 \times \kappa^2 \times V^2}}, \tag{6}$$

Since the physiological variance is not from true thermal noise processes, it could be partly removed if its origin and its behavior was better understood. Several methods have utilized physiological monitoring of the cardiac and respiratory cycle to try to reduce the physiological signal clutter from the fMRI time-course (Glover et al., 2000; Le et al., 1996; Pfeuffer et al., 2002; Thomas et al., 2002).

Previous studies (Krueger et al., 2001) have demonstrated an asymptotic relationship between the variance in the SNR time-course and the thermal image noise at a fixed moderate spatial resolution at field strengths of 1.5 T and 3 T. A major concern raised by this work was that additional increases in sensitivity afforded by higher field strengths were not expected to translate to significant improvements in the time-course SNR. In this paper, we examine the effects of the magnetic field strength on the physiological noise at 1.5 T, 3 T, and 7 T. In addition, we extended previous observations to higher spatial resolutions, where thermal image noise dominates the time-course variance and thus alters the effective tradeoff between image SNR and time-course SNR. In this high spatial resolution regime, increases in image SNR gained by use of the 7 T system still translate to substantially improved time-course SNR.

Methods

Comparative studies were performed at three different field strengths on a Siemens Sonata 1.5 T whole body system, Allegra 3 T head-only scanner and a prototype 7 T head-only system (Siemens Medical Solutions, Erlangen Germany). The same 8 healthy volunteers were scanned on the 1.5 T and 3 T imagers, another 8 healthy volunteers were imaged on the 7 T scanner. Resolution dependence was studied in 5 of these subjects and flip angle dependence was studied in the other 3. The TE dependence of the noise was studied in an additional 2 subjects. Written consent was obtained from all the subjects under protocols approved by institutional review. Head immobilization was achieved with foam pads and subjects were asked to relax while in the scanner; no specific stimulus was applied. Commercial volume head coils were used on the 1.5 T and 3 T systems, while an in-house made end-capped TEM volume head coil was used at 7 T.

Data acquisition

In setting the scan parameters on the 3 different scanners, we chose to optimize the EPI scan on the particular gradient hardware available at that field strength rather than standardize to the lowest common denominator for TE, EPI readout bandwidth and echo spacing. To study the effect of flip angle on time-course SNR, single shot, fully relaxed gradient echo EPI images were collected with flip angles of 12°, 24°, 37°, 53°, 90° using TR = 5400 ms, three 4-mm-thick slices with a 2-mm slice gap, 60 time points, FOV = 240 × 240 mm^2, matrix = 128 × 128, and a TE of 40 ms, 30 ms, and 20 ms for 1.5 T, 3 T and 7 T, respectively. The bandwidth and echo spacing were, respectively 2298 Hz/pixel and 0.55 ms for 1.5 T, 2604 Hz/pixel and 0.43 ms for 3 T, and 2790 Hz/pixel and 0.4 ms for the 7 T. The same TR and number of time-points were used to study the effect of spatial resolution but with a flip angle of 90°, ten 3 mm thick slices with 3 mm slice gaps and spatial resolutions of 1 × 1 × 3 mm^3, 1.5 × 1.5 × 3 mm^3, 2 × 2 × 3 mm^3, 3 × 3 × 3 mm^3, 4 × 4 × 3 mm^3, and 5 × 5 × 3 mm^3. The FOV, image matrix, TE, degree of partial Fourier encoding, readout bandwidth (BW) and echo spacing used are shown in Tables 1a, 1b and 1c for 1.5 T, 3 T, and 7 T, respectively. In all cases, images at flip angle 0° were also obtained to determine the thermal image noise. For comparison, time series data using these same parameters were also acquired on a loading phantom.

To study the "BOLD noise" contribution, the image time course variance was studied by varying the TE of the EPI sequence at 3 T and 7 T. Resolutions of 2 × 2 × 3 mm^3, 3 × 3 × 3 mm^3, 4 × 4 × 3 mm^3 were acquired with TR = 3000 ms, 10 slices. A multi-echo EPI sequence with an acquisition of 6 echoes was used for the lower spatial resolutions and a 3-echo train for the higher spatial resolution. Multiple runs were acquired to obtain time series with echo times of 15 ms, 20 ms, 25 ms 30 ms, 35 ms, 40 ms, 50 ms, and 60 ms at 7 T and 20 ms, 25 ms, 30 ms, 40 ms,

Table 1a
Acquisition parameters for the acquired EPI resolutions at 1.5 T

Resolution (mm^3)	FOV (mm^2)	Matrix	TE (ms)	Partial Fourier	BW (Hz/px)	Echo Spacing (ms)
1 × 1 × 3	192 × 192	192 × 192	46	6/8	1302	0.83
1.5 × 1.5 × 3	192 × 192	128 × 128	40	6/8	2056	0.62
2 × 2 × 3	256 × 256	128 × 128	40	6/8	2298	0.53
3 × 3 × 3	192 × 192	64 × 64	40	8/8	3256	0.43
4 × 4 × 3	256 × 256	64 × 64	40	8/8	3720	0.37
5 × 5 × 3	320 × 320	64 × 64	40	8/8	3720	0.34

50 ms, 60 ms, 70 ms, 80 ms 90 ms, and 100 ms at 3 T. In all cases, images at flip angle 0° were also obtained to determine the thermal image noise.

Data analysis

To reduce the effect of head movements, image registration within each time series was performed using the AFNI motion correction software (Cox and Jesmanowicz, 1999). Linear and quadratic trends in the image intensity were also removed from the time-course. The SNR in an individual image (SNR_0) and the SNR derived from the image-to-image variance in the time-course (tSNR) were measured in ROIs defined in cortical gray matter. SNR_0 for a given pixel was calculated as the mean pixel value for all the images in the time-series divided by the standard deviation of the thermal noise of the time-series acquired with no RF excitation (zero flip angle images). This value was then used to estimate the standard deviation of the underlying Gaussian distribution of the original complex data using the relation $\sigma_{complex} = 1.527\ \sigma_{magnitude}$ (Gudbjartsson and Patz, 1995).

Temporal SNR (tSNR) in a given pixel was determined from the mean pixel value across the 60 time points divided by its temporal standard deviation. Since all of the images had SNR above 10 in the brain, the Rician distribution of the magnitude data is well approximated as a Gaussian distribution. The maps of SNR_0 and tSNR were then reduced to a single number for a given set of acquisition parameters through ROI analysis. The ROI included regions from each of the slices including frontal, parietal and occipital gray matter.

For the set of flip angles or the set of spatial resolutions, the tSNR was analyzed as a function of SNR_0. The tSNR as a function of SNR_0 was fit to Eq. (5), using a non-linear least squares minimization algorithm provided by Matlab (Mathworks, Natick, USA) with λ as a free parameter. For an image time course at a given spatial resolution and flip angle, the ratio of physiological to thermal noise was computed from Eq. (3). The relationship between tSNR and voxel volume was fit using Eq. (6) with 2 free parameters λ and κ.

The relative contribution of the BOLD and non-BOLD component of the physiological noise was determined by measuring SNR_0 and tSNR at different TE values. Firstly, T2* maps were generated on a pixel by pixel basis from the echo time data. T2* values were then averaged over the gray matter ROIs. For each TE, a λ was determined by non-linear least squares fitting of Eq. (5) using the 3 spatial resolutions. The measured λ^2 as a function of TE was fit to a linear function, the slope and intercept of which determined σ_B and σ_{NB}, respectively. The ratio of σ_B to σ_0 was plotted as a function of echo time and fit using the measured T2* values and $\sigma_B = c_1 \times \Delta R_2^* \times \mathrm{TE} \times S_0 \times e^{-\mathrm{TE/T2^*}}$.

Results

Physiological noise and flip angle modulation

Fig. 1 shows the tSNR as a function of SNR_0 when SNR_0 is modulated by the flip angle at a fixed spatial resolution (1.9 × 1.9 × 4 mm^3). Results from all three field strengths are illustrated, with squares, circles and diamonds representing the 1.5 T, 3 T and 7 T data, respectively. As SNR_0 is increased with higher flip angles, an asymptotic behavior is observed at the higher field strengths (3 T and 7 T). Table 2 presents the corresponding mean values and standard deviation as obtained from all three subjects. Physiological noise was the dominant noise source at higher field strengths (3 T and 7 T) for the higher flip angle scans. For the low flip angle acquisitions, the thermal image noise dominated at all field strengths for this image resolution. For example, at a flip angle of 37°, the ratio of the physiological over thermal noise determined from Eq. (3) is 0.25 ± 0.31, 0.46 ± 0.28 and 0.66 ± 0.10 for 1.5 T, 3 T and 7 T, respectively, while at 90° flip angle, which corresponds to the highest MR signal and thus the highest physiological noise, this ratio increased to 0.80 ± 0.06, 1.06 ± 0.09 and 1.65 ± 0.08. The λ values as estimated using the non-linear least squares fitting algorithm (Matlab, Natick MA) with lower and upper 95% confidence limits stated in the parenthesis were λ = 0.0123 (0.0046 and 0.0201), λ = 0.0107 (0.0099 and

Table 1b
Acquisition parameters for the acquired EPI resolutions at 3 T

Resolution (mm^3)	FOV (mm^2)	Matrix	TE (ms)	Partial Fourier	BW (Hz/px)	Echo spacing (ms)
1 × 1 × 3	192 × 192	192 × 192	41	6/8	1532	0.70
1.5 × 1.5 × 3	192 × 192	128 × 128	30	6/8	2298	0.51
2 × 2 × 3	256 × 256	128 × 128	30	6/8	2790	0.40
3 × 3 × 3	192 × 192	64 × 64	30	8/8	4112	0.31
4 × 4 × 3	256 × 256	64 × 64	30	8/8	4882	0.27
5 × 5 × 3	320 × 320	64 × 64	30	8/8	4882	0.24

Table 1c
Acquisition parameters for the acquired EPI resolutions at 7 T

Resolution (mm^3)	FOV (mm^2)	Matrix	TE (ms)	Partial Fourier	BW (Hz/px)	Echo spacing (ms)
1 × 1 × 3	192 × 192	192 × 192	39	6/8	1532	0.70
1.5 × 1.5 × 3	192 × 192	128 × 128	20	6/8	2298	0.51
2 × 2 × 3	256 × 256	128 × 128	20	6/8	2790	0.40
3 × 3 × 3	192 × 192	64 × 64	20	8/8	4112	0.31
4 × 4 × 3	256 × 256	64 × 64	20	8/8	4112	0.29
5 × 5 × 3	320 × 320	64 × 64	20	8/8	4882	0.25

0.0115), and $\lambda = 0.0086$ (0.0079 and 0.0094) for 1.5 T, 3 T and 7 T, respectively indicating that at this image resolution the asymptotic limit for tSNR ($1/\lambda$) was 81.3, 93.5 and 116.3.

Physiological noise and image resolution

Fig. 2 shows the image SNR (SNR_0) as a function of voxel volume for the 3 different field strengths. As expected, the SNR_0 is nearly linear in voxel volume and at each resolution SNR_0 increases approximately linearly with field strength. Fig. 3 shows tSNR as a function of SNR_0 as the image resolution is varied. Again, squares, circles, and diamonds represent the field strengths of 1.5 T, 3 T, and 7 T, respectively. Similarly to the flip angle measurement, tSNR displayed an asymptotic behavior with increasing SNR_0.

The free parameter λ from Eq. (5) was determined from the fit with lower and upper 95% confidence limits stated in the parenthesis to be $\lambda = 0.0109$ (0.0102 and 0.0117), 0.0111 (0.0104 and 0.0119), and $\lambda = 0.0113$ (0.0102 and 0.0123), for 1.5 T, 3 T, and 7 T field strengths suggesting an asymptotic maximum ($1/\lambda$) for tSNR of 91.7, 90.1, 88.5 for the three field strengths. Similarly, the fit of Eq. (5) to all the human data gave λ equal to 0.0112 (lower and upper 95% confidence limits equal to 0.0108 and 0.0116). Fig. 4 shows a similar study of tSNR as a function of SNR_0 in the phantom data. For comparison, the curve determined by fitting the human data is shown in Fig. 4 as dashed lines. At all resolutions, the phantom tSNR was considerably higher than the human tSNR. A slight deviation from the identity line is observed in the phantom data, perhaps due to shot-to-shot gain variations in the scanner, which would have the same functional dependence on image signal as we have assumed for the physiological noise. The λ determined from the phantom data was 0.00075 (lower and upper 95% confidence limits equal to 0.00068 and 0.00081), corresponding to an asymptotic limit for tSNR ($1/\lambda$) of 1333, approximately 15-fold higher than in vivo.

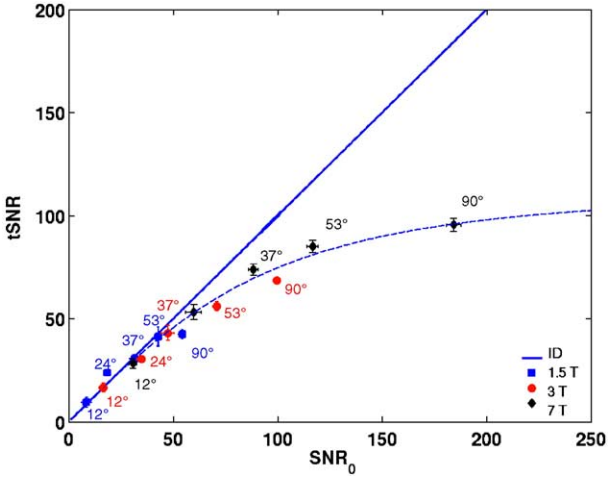

Fig. 1. SNR in fMRI time series (tSNR) as a function of image SNR (SNR_0) at a constant resolution of 1.9 × 1.9 × 4 mm^3. Labels indicate flip angle of the measurement. Each point represents the average from areas of cortical gray matter over three subjects. The solid line represents the line of identity (tSNR = SNR_0), and the dashed line is the model fit (Eq. (5)) to all the data points. Residuals between the measured data and model fit show an approximate random scatter of the measured data above and below the fit with relatively small total residual indicating an adequate goodness of fit.

Table 3 shows the average SNR_0 and tSNR values from the five subjects for each field strength as well as the computed σ_p/σ_0 (from Eq. (3)). Fig. 5 shows the physiologic to thermal noise ratio as a function of voxel volume for each of the three field strengths. At a given spatial resolution, the ratio of physiological noise to thermal noise always increased with field strength. Although the higher field strengths showed a higher physiological to thermal noise ratio, the higher field strengths also showed a steeper decline in this ratio with voxel volume. Although the physiological noise dominated tSNR at the higher field strengths and larger voxel volumes, it was possible to obtain thermal noise dominated images ($\sigma_p/\sigma_0 < 1$) at all field strengths. When the spatial resolution was high enough to assure that the time course was dominated by thermal image noise, improvements in SNR from improved RF coil design or even higher field strengths are likely to translate into improved time-course SNR.

Fig. 6 shows tSNR plotted as a function of voxel volume for the three field strengths. At each field, tSNR increased monotonically with voxel volume, but the largest gains in tSNR as a function of voxel size occurred at the highest spatial resolution. At coarser spatial resolutions, all three field strengths showed asymptotic behavior, with the higher field strengths nearing the asymptote at smaller voxel volumes. From the fit data and assuming a linear relationship between SNR_0 and voxel volume, we expect that tSNR obtains 80% of its asymptotic maximum ($1/\lambda$) at a resolution of 28.6 mm^3, 15.0 mm^3, 11.7 mm^3 for 1.5 T, 3 T, and 7 T, respectively. Fig. 7 shows the ratio gain of tSNR obtained from going to higher field strength. The ratio of tSNR(7 T)/tSNR(3 T), tSNR(3 T)/tSNR(1.5 T), and of tSNR(7 T)/tSNR(1.5 T) are plotted as a function of voxel volume. Except for the highest resolution data sets, these ratios were all monotonically increasing with image resolution.

The multi TE measurements yielded a T2* for the gray matter ROI of 51 ms at 3 T and 30 ms at 7 T. Fig. 8 shows the measured BOLD-like component of the physiologic noise as a function of TE for 3 T and 7 T. The observed TE dependence was well described by the expected BOLD contrast function with maximum BOLD

Table 2
Average values ± standard deviations for SNR measurements obtained from 3 normal subjects, as a function flip angle and field strength for a spatial resolution of 1.9 × 1.9 × 4 mm^3

Flip angle (°)	7 T			3 T			1.5 T		
	SNR_0	tSNR	σ_p/σ_0	SNR_0	tSNR	σ_p/σ_0	SNR_0	tSNR	σ_p/σ_0
12	30.68 ± 1.9	28.12 ± 2.3	0.44 ± 0.28	16.56 ± 1.9	16.45 ± 2.1	0.11 ± 1.51	8.48 ± 2.3	9.43 ± 2.5	–
24	59.76 ± 3.8	53.09 ± 3.6	0.52 ± 0.23	34.72 ± 2.0	30.28 ± 1.6	0.56 ± 0.18	18.41 ± 1.4	23.87 ± 1.5	–
37	88.43 ± 2.4	73.74 ± 2.8	0.66 ± 0.10	47.40 ± 3.1	43.03 ± 3.6	0.46 ± 0.28	31.54 ± 2.3	30.60 ± 1.9	0.25 ± 0.31
53	116.85 ± 2.7	85.00 ± 3.0	0.94 ± 0.08	70.74 ± 1.7	56.00 ± 2.1	0.77 ± 0.09	42.82 ± 1.8	41.37 ± 4.6	0.27 ± 0.17
90	184.19 ± 3.5	95.40 ± 3.1	1.65 ± 0.08	99.70 ± 1.2	68.48 ± 1.3	1.06 ± 0.09	54.37 ± 1.7	42.38 ± 2.1	0.80 ± 0.06

Image SNR (SNR_0) corrected for Rayleigh distribution.

noise near T2*. Like the total physiological noise, the BOLD-like component increased relative to σ_0 for larger voxel volumes and higher field strength. For a 7 T experiment optimized with TE = T2*, the ratio of σ_B to σ_0 was 0.46 ± 0.03, 0.64 ± 0.01 and 1.30 ± 0.04 for 12 mm^3, 27 mm^3 and 48 mm^3 voxel volumes. For 3 T, the percentage contribution of BOLD noise was lower: 0.33 ± 0.01, 0.43 ± 0.02, and 0.74 ± 0.01 for the same resolutions.

The non-BOLD noise component of the physiological noise also increased with the field strength. At 7 T with TE = 30 ms (the measured TE closest to the observed $T2^*$), the ratio of the σ_{NB} to σ_0 was 0.023 ± 0.001, 0.031 ± 0.001 and 0.062 ± 0.002 for voxel size of 12 mm^3, 27 mm^3, and 48 mm^3, respectively. Similarly, at 3 T with TE = 50 ms, the σ_{NB} to σ_0 ratio was 0.013 ± 0.001, 0.017 ± 0.001 and 0.029 ± 0.003 for voxel size of 12 mm^3, 27 mm^3, and 48 mm^3, respectively.

Discussion

In this work, we examined the effects of the magnetic field strength, flip angle, image resolution, and TE on the physiological noise and corresponding SNR in the functional imaging time-course. We extend earlier investigations (Krueger and Glover, 2001; Krueger et al., 2001) on the physiological noise in fMRI by increasing the field strength to 7 T and studying the effect of voxel volume. Results agreed with previous work in that the relationship between tSNR and SNR_0 was parameterized by a similar λ in gray matter (current study: λ = 0.010, literature: λ = 0.012 (Krueger and Glover, 2001)). The model for tSNR (Krueger and Glover, 2001) thus appears to hold when image SNR is modulated by increased field strength (7 T) and voxel volume.

The fMRI time-course SNR is observed to be near its asymptotic limit for conventional spatial resolutions at 3 T and 7 T. When the previous work is extrapolated to the higher SNR_0 expected from 7 T, tSNR was expected to be limited by physiological noise. Our study demonstrates this effect. However, when higher spatial resolutions were examined, the limitations in tSNR from physiological noise were significantly mitigated. For example, at a voxel volume of 44.5 mm^3, 18.2 mm^3 and 3.0 mm^3 for 1.5 T, 3 T and 7 T, respectively, the ratio of physiologic to thermal noise is expected to be 0.9, thus, the time-course SNR was dominated by image noise and not physiological noise. At smaller voxel volumes, the fMRI experiment is not near the asymptotic limit of tSNR and the improvements in image SNR are expected to translate into significant improvements in tSNR. For example, the relative improvement seen from moving to higher field strength (as expressed in Fig. 7, by the tSNR(7 T)/tSNR(3 T) and tSNR(7 T)/

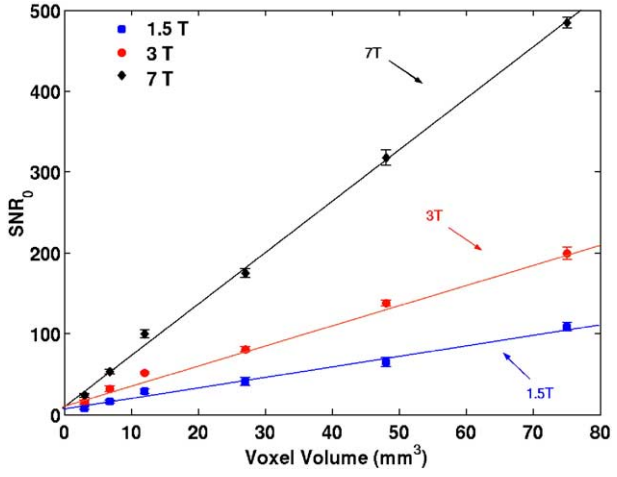

Fig. 2. Image SNR (SNR_0) as a function of voxel volume. Measurements derived from areas of cortical gray matter and are averages over five subjects at each field strength. Lines are linear least-squares fit to the data. SNR_0 was normalized for bandwidth differences and differences in the degree of partial Fourier acquisition.

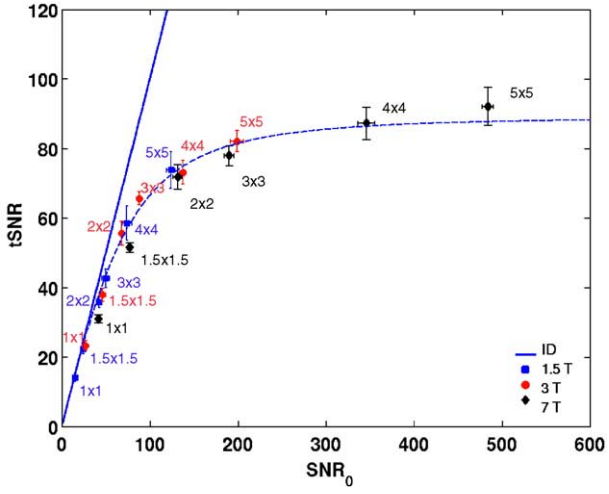

Fig. 3. SNR in fMRI time series (tSNR) as a function of image SNR (SNR_0) for different spatial resolutions. Changes in SNR were produced by varying the voxel volume. Labels indicate the in-plane resolution in mm^2 at 3 mm slice thickness. Measurements derived from areas of cortical gray matter and are averages over five subjects at each field strength. The solid line represents the line of identity (tSNR = SNR_0), and the dashed line shows the model fit (Eq. (5)) to all the data points. Residuals between the measured data and model fit show an approximate random scatter of the measured data above and below the fit with relatively small total residual indicating an adequate goodness of fit.

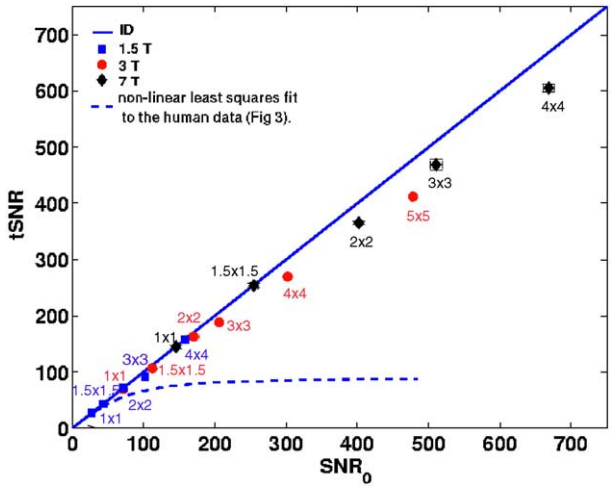

Fig. 4. tSNR as a function of image SNR_0 in a phantom (data points) for different spatial resolutions and field strengths. Labels indicate the in-plane resolution in mm^2 at 3 mm slice thickness. The solid line corresponds to the line of identity (tSNR = SNR_0) and the dashed line shows the non-linear least squares fit to the corresponding human data of Fig. 3.

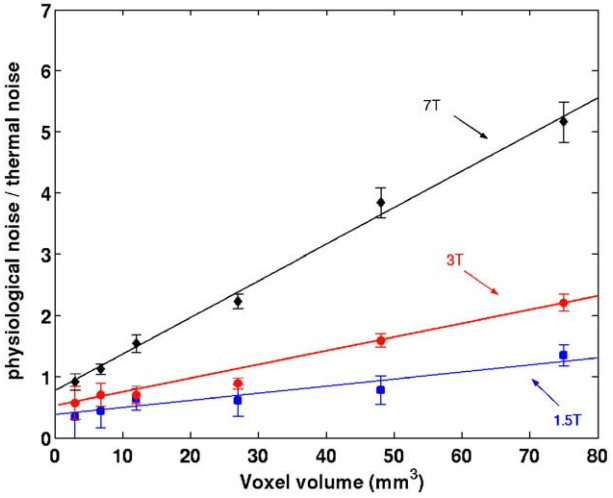

Fig. 5. Ratio of physiological to thermal noise as a function of voxel volume. Measurements derived from areas of cortical gray matter and are averages over five subjects at each field strength.

tSNR(1.5 T) ratios) was seen to increase with higher image resolution. However, the monotonic increase in these ratios was not observed in the highest spatial resolution data, a deviation which might have been due to the fact that TE was increased to accommodate this resolution. The increased T2* weighting and/or the increased T2* blurring might have altered the relative physiological noise content in this data set. At a given spatial resolution, the ratio of physiological noise to thermal noise always increased with field strength. Although the higher field strengths showed a higher physiological to thermal noise ratio, the higher field strengths also showed a steeper decline in this ratio with voxel volume.

In this study, we only analyze SNR effects and do not address potential contrast benefits from higher field or contrast-to-noise benefits from improved partial volume effects at higher spatial resolution. This study does not consider the effect of physiological monitoring with the goal of removing sources of time course variance (Glover et al., 2000; Le et al., 1996). If these strategies are effectively performed, the time-course SNR will be reduced placing it closer to the thermal limit. This should allow lower spatial resolution acquisitions to also benefit from higher field strength and improved RF detectors. In addition, the removal of linear and quadratic trends from the fMRI time-course in the current study might also partly remove physiological noise. Other studies have also used the physiological noise correlations to try to assess functional connectivity between brain regions (Biswal et al., 1995). In this case, the increased physiological to thermal noise ratio observed in our data at 7 T should facilitate this type of study.

The acquisition parameters for each spatial resolution were selected based on the practical tradeoffs between TE, BW, and echo spacing. In general, we tried to use realistically optimized fMRI acquisition parameters at each field strength and utilize the maximum gradient performance of each system to minimize susceptibility distortions in the image rather than choosing the lowest common denominator for all field strengths. Although, imaging parameters such as BW and degree of partial Fourier acquisition effect SNR_0, they do so in a predictable way. Also, since most of the conclusions were obtained from a comparison of tSNR to SNR_0, the conclusions are insensitive to these differences. There is the possibility that the results were skewed by the choice of TE at each field strength; we attempted to use commonly chosen TE values motivated by CNR and susceptibility artifact considerations to make the conclusions more practically relevant. This choice of TE was also validated by the TE dependency study which showed that the BOLD-like physiological noise component peaked at a TE near the TE used for the other studies.

In our study, σ represents the total noise in the time series which originates from the combination of thermal noise from the subject coil and preamp (σ_0) as well as physiological fluctuations in the image signal intensity (σ_p). In the treatment by Krueger and Glover (2001), scanner instabilities were labeled as part of σ_0 but not explicitly isolated for study. If the amplitude of physiological

Table 3
Average values ± standard deviations for SNR measurements from 5 normal subjects, as a function of image resolution and field strength

Resolution (mm^3)	7 T			3 T			1.5 T		
	SNR_0	tSNR	σ_p/σ_0	SNR_0	tSNR	σ_p/σ_0	SNR_0	tSNR	σ_p/σ_0
1 × 1 × 3	41.70 ± 2.15	30.90 ± 1.12	0.91 ± 0.13	26.78 ± 2.66	23.31 ± 1.43	0.57 ± 0.27	14.98 ± 1.62	14.18 ± 1.13	0.34 ± 0.4
1.5 × 1.5 × 3	77.33 ± 2.64	51.43 ± 1.32	1.12 ± 0.09	46.33 ± 3.46	37.94 ± 1.86	0.70 ± 0.19	24.30 ± 1.84	22.36 ± 1.41	0.43 ± 0.2
2 × 2 × 3	131.70 ± 5.07	71.80 ± 3.62	1.54 ± 0.14	67.98 ± 1.58	55.63 ± 3.43	0.70 ± 0.14	42.44 ± 2.79	35.87 ± 1.66	0.63 ± 0.1
3 × 3 × 3	190.29 ± 5.38	77.95 ± 2.86	2.23 ± 0.12	87.80 ± 3.19	65.62 ± 1.90	0.89 ± 0.09	49.98 ± 4.73	42.67 ± 2.71	0.61 ± 0.2
4 × 4 × 3	346.17 ± 9.66	87.23 ± 4.62	3.84 ± 0.25	137.51 ± 3.52	73.14 ± 3.28	1.59 ± 0.11	74.19 ± 5.41	58.53 ± 4.93	0.78 ± 0.2
5 × 5 × 3	484.21 ± 6.67	92.06 ± 5.44	5.16 ± 0.33	199.14 ± 7.52	82.09 ± 3.04	2.21 ± 0.14	123.95 ± 5.02	73.85 ± 5.28	1.35 ± 0.1

SNR_0 corrected for Rayleigh distribution.

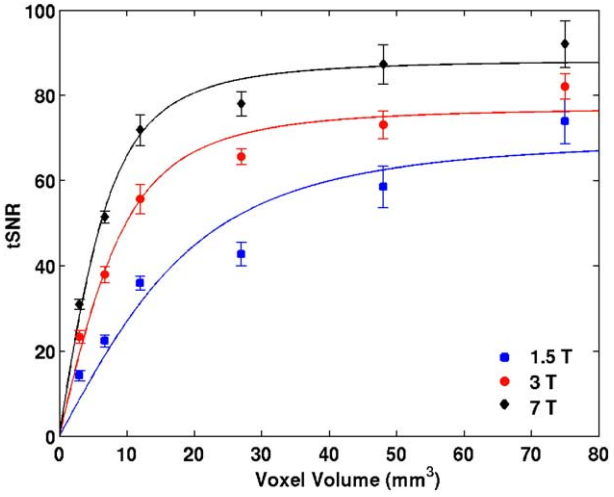

Fig. 6. Time-course SNR (tSNR) as a function of voxel volume. Measurements derived from areas of cortical gray matter and are averages over five subjects at each field strength. The solid lines represent fit of Eq. (6) to the data.

noise is modeled as a modulation of the image intensity ($\sigma_p \propto S$), then the model will also include any scanner instability with this signal dependence within the measure of σ_p. In this work, we do not attempt to separate scanner instability into σ_0 or σ_p, but note that in our measurements both σ_0 or σ_p will contain some sources of variance from shot to shot instabilities in the scanner hardware, such as gradient induced preamplifier gain fluctuations, or transmit amplitude variations. By measuring the time-course fluctuations in a phantom study, we note that the variance from scanner instabilities is small compared to the in vivo fluctuations. Therefore, the nomenclature error in referring to σ_p as "physiological" is a minor one.

Scanner instabilities which have no signal dependence will contribute to σ_0 in our measurement of phantom SNR. These instabilities will not contribute to an asymptotic behavior in the plot

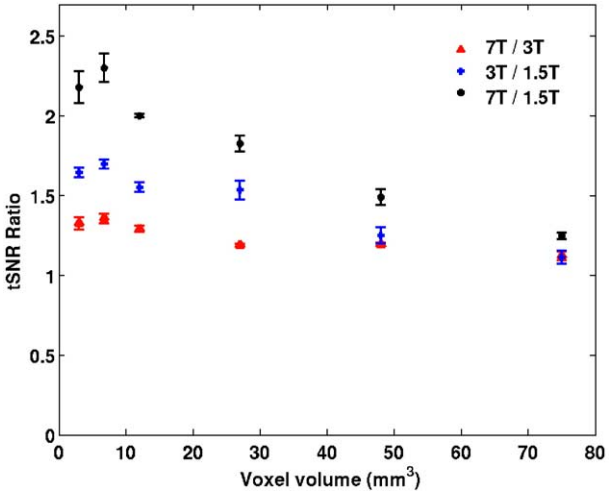

Fig. 7. Ratio of the time-course SNR (tSNR) at different field strengths as a function of voxel volume. The ratios of 7 T to 1.5 T, 3 T to 1.5 T, and 7 T to 3 T are illustrated with stars, crosses and triangles, respectively. Measurements derived from areas of cortical gray matter and are averages over five subjects at each field strength.

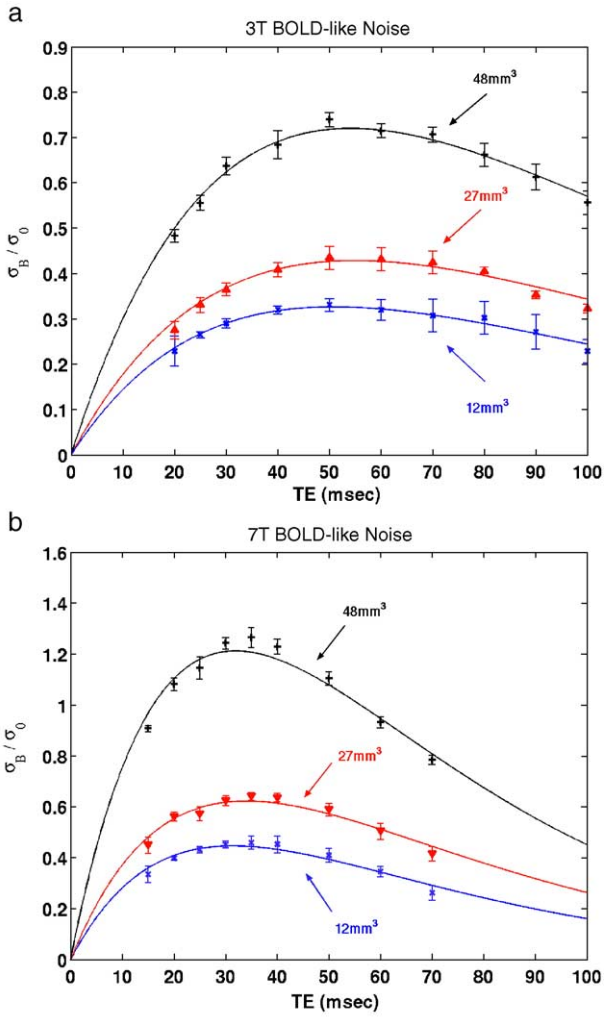

Fig. 8. Ratio of BOLD-like physiological noise component to thermal noise for 12 mm^3 (crosses), 27 mm^3 (triangles), and 48 mm^3 (pluses) and fit to noise model (solid lines) at 3 T (a) and 7 T (b).

of tSNR versus SNR_0 for the phantom since their signal dependence is the same as thermal image noise. The inability to achieve asymptotic behavior in the phantom plot of tSNR versus SNR_0 shows that the scanner variance due to the signal independent instabilities and thermal noise dominates variance which is proportional to the signal. In most cases, Weisskoff (1996) tests of scanner instabilities show that with sufficient spatial smoothing of the phantom images, an asymptotic behavior is reached.

Conclusion

This work verifies that the temporal SNR of the fMRI experiment reaches a plateau at high image SNR. However, we only analyze SNR effects and ignore potential contrast benefits from higher field or contrast-to-noise benefits from improved partial volume effects at higher spatial resolution. For our studies, once the image SNR (with Rayleigh correction) reached an SNR of ~100, further improvements in image SNR are expected to yield only marginal increases in the time-course SNR. At high image resolutions, however, the image SNR is reduced to a point where

the time-course SNR was not dominated by physiological noise. The higher resolution experiments were shown to have the potential to benefit significantly from the use of field strengths of 7 T and above. Although the physiological noise dominated tSNR at larger voxel volumes and higher field strengths, it was possible to obtain thermal noise dominated images ($\sigma_p/\sigma_0 < 1$) at all field strengths. When the spatial resolution was high enough to assure that the time course was dominated by thermal image noise, improvements in SNR from improved RF coil design or even higher field strengths are likely to translate into improved time-course SNR.

Acknowledgments

The authors would like to thank the Office of National Drug Control Policy (ONDCP), Counterdrug Technology Assessment Center, the National Institute of Health Grants P41 RR14075 and RO1 RR14543 A01, and the Mental Illness and Neuroscience Discovery Institute (MIND). We thank Mark Vangel, Ph.D., for his helpful discussions concerning error analysis.

References

Bandettini, P.A., Wong, E.C., Jesmanowicz, A., Prost, R., Cox, R.W., Hinks, R.S., Hyde, J.S., 1994. MRI of human brain activation at 0.5 T 1.5 T, and 3.0 T: comparison of ΔR_2^* and functional contrast to noise ratio. Proc. ISMRM, 434.

Biswal, B., Yetkin, F.Z., Haughton, V.M., Hyde, J.S., 1995. Functional connectivity in the motor cortex of resting human brain using echo-planar MRI. Magn. Reson. Med. 34, 537–541.

Cox, R.W., Jesmanowicz, A., 1999. Real-time 3 D image registration for functional MRI. Magn. Reson. Med. 42, 1014–1018.

Edelstein, W.A., Glover, G.H., Hardy, C.J., Redington, R.W., 1986. The intrinsic signal-to-noise ratio in NMR imaging. Magn. Reson. Med. 3, 604–618.

Fera, F., Yongbi, M.N., van Gelderen, P., Frank, J.A., Mattay, V.S., Duyn, J.H., 2004. EPI-BOLD fMRI of human motor cortex at 1.5 T and 3.0 T: sensitivity dependence on echo time and acquisition bandwidth. J. Magn. Reson. Imaging 19, 19–26.

Gati, J.S., Menon, R.S., Ugurbil, K., Rutt, B.K., 1997. Experimental determination of the BOLD field strength dependence in vessels and tissue. Magn. Reson. Med. 38, 296–302.

Glover, G.H., Li, T.Q., Ress, D., 2000. Image-based method for retrospective correction of physiological motion effects in fMRI: RETROICOR. Magn. Reson. Med. 44, 162–167.

Gudbjartsson, H., Patz, S., 1995. The Rician distribution of noisy MRI data. Magn. Reson. Med. 34, 910–914.

Krueger, G., Glover, G.H., 2001. Physiological noise in oxygenation-sensitive magnetic resonance imaging. Magn. Reson. Med. 46, 631–637.

Krueger, G., Kastrup, A., Glover, G.H., 2001. Neuroimaging at 1.5 T and 3.0 T: comparison of oxygenation-sensitive magnetic resonance imaging. Magn. Reson. Med. 45, 595–604.

Le, T.H., Hu, X., 1996. Retrospective estimation and correction of physiological artifacts in fMRI by direct extraction of physiological activity from MR data. Magn. Reson. Med. 35, 290–298.

Matlab Mathworks Inc., Natick, U.S.A.

Pfeuffer, J., Van de Moortele, P.F., Ugurbil, K., Hu, X., Glover, G.H., 2002. Correction of physiologically induced global off-resonance effects in dynamic echo-planar and spiral functional imaging. Magn. Reson. Med. 47, 344–353.

Thomas, C.G., Harshman, R.A., Menon, R.S., 2002. Noise reduction in BOLD-based fMRI using component analysis. NeuroImage 17, 1521–1537.

Turner, R., Jezzard, P., Wen, H., Kwong, K.K., Le Bihan, D., Zeffiro, T., Balaban, R.S., 1993. Functional mapping of the human visual cortex at 4 and 1.5 Tesla using deoxygenation contrast EPI. Magn. Reson. Med. 29, 277–279.

Weisskoff, R.M., 1996. Simple measurement of scanner stability for functional NMR imaging of activation in the brain. Magn. Reson. Med. 36, 643–645.

Weisskoff, R.M., Baker, J., Belliveau, J., Davis, T.L., Kwong, K.K., Cohen, M.S., Rosen, B.R., 1993. Power spectrum analysis of functionally-weighted MR data: what's in the noise? Proc. ISMRM, 7.